10th International Symposium on Practical Design of Ships and Other Floating Structures
Houston, Texas, United States of America

Mesh Size Effects in Simulating Ductile Fracture of Metals

Y. N. Li [1)], D. G. Karr [1)], G. Wang [2)]

[1)] University of Michigan, 2600 Draper Rd., Ann Arbor MI, 48109-2145
[2)] American Bureau of Shipping, 16855 Northchase Drive, Houston TX, 77060-6008

Presented at PRADS 2007, Houston, TX, USA, 1-5 October 2007 and reprinted with the kind permission of the 10th International Symposium on Practical Design of Ships and Other Floating Structures (PRADS)

Abstract

Physical scale and size effects influence the failure of structures and structural components. This can be especially true when failure is due to brittle, quasi-brittle, or ductile fracture. When simulating ductile fracture using the finite element method, mesh size effects are also encountered. A common approach for analyzing the response of hull structures due to grounding and impact, for example, is to eliminate elements or to allow elements to split when a critical strain to failure is achieved. However, an important complication arises because of the observed mesh size sensitivity whereby strain to failure generally increases with finer finite element meshes. In this paper we explore the relation between the critical strain to failure, ε_f , and the size of the "unit cell" or finite element. Our study focuses on applications for marine structures involving fracture of metals including, for example, aluminum, magnesium, and steel alloys. Extensions to two and three dimensional stress states are also discussed.

Keywords

Size effects; Ductile fracture; Bifurcation; Simulation.

Introduction

The study of size effects has a long history since Leonardo da Vinci, and interest in this topic has risen over recent decades due to the development of advanced simulation capability, particularly finite element analysis. Both deterministic and statistical aspects of scaling can influence structural and material failure theories (Bažant, 1997, 2000). The present study focuses on developing a deterministic methodology to predict mesh size effects for ductile fracture.

When simulating ductile fracture using the finite element method, mesh size effects are encountered. It is common that finer mesh sizes are needed for better results when spacial gradients of deformation are high. However, this is not necessarily true when one encounters simulation processes in which material failure is significant as in, for example, impact, explosion, implosion, ship grounding, and sheet metal forming studies (Kuroiwa, Kawamoto and Yuhara, 1992, Kitamura, 2001, Servis, Samuelides, Louka and Voudouris, 2001). For such large scale simulations, a common approach for analyzing the response of hull structures due to grounding and impact, for example, is to eliminate elements (Li 2002) or to allow elements to split (Simonsen and Tornqvist., 2004) when a critical strain to failure is achieved. However, an important complication arises because of the observed mesh size sensitivity whereby strain to failure generally increases with finer finite element meshes.

For decades, researchers found the value of strain to failure is mesh-dependent and attempts were made to find their relation, although the results are for the most part based on empirical relationships. For example, the International Ship and Offshore Structures Congress reviewed the state-of-the-art of rupture strain in research on ships' collision and grounding (Wang et al. 2006), and organized a series of benchmark studies to compare some formulae (Paik et al. 2003). Lehmann and Yu (1998) presented an empirical power law model to handle the tri-axial rupture criteria, and it was improved by Broekhuijsen (2003). The range of critical values of rupture strain was studied by Okazawa et al (2004), Yamada et al (2005), and Alsos and Amdahl (2005). Other efforts, with particular emphasis on failure of aluminum, are reported by Lee and Wierzbicki (2005). In this investigation, it is argued that mesh-size dependence can be determined by the constitutive relations and the microscale imperfections of the material, either geometric or material. Although theoretical studies of size effects are presented, notably Bažant and Guo (2002), and Engelen et al. (2006) using strain-gradient theory (Fleck and Hutchinson,1993, 2001), there still are gaps between the theory and industrial application. The purpose of this study is to explain size effects physically and present a methodology to predict size effects for marine structures involving ductile fracture of metals including aluminum, magnesium, and steel alloys.

Damage and fracture models of various complexities consider the nucleation, growth and coalescence of voids in a homogenous matrix such as the classical references by McClintock (1968, 1971), Rice and Tracey (1969), Gurson

(1977), and Needleman and Tvergaard (1984). Implementation of plasticity and damage models in finite element codes often involves the use of a material characteristic length or involves explicitly modeling the micro structural features. In the present study, this kind of constitutive model is also used together with the simplified power law plasticity model. Initiating from the one dimensional analysis, extensions to two and three dimensional stress states are also discussed.

Problem Formulation

An intuitional idea about size effect is shown in Fig. 1 qualitatively. It is obvious that the average strain in mesh 2 is larger than that in mesh 1, at the time when fracture is occurring. In fact, within subsets of mesh 2, facture is in fact complete; a continuum description of the strain in such zones leads to infinite strains. To study size effects quantitatively, a simplified three-piece-cell, shown in Fig. 2, is used (Li and Karr 2007(a)) representing a typical unit cell or single finite element. Different from typical finite element descriptions with homogeneous stress and strain, it has an imperfect part and allows strain localization. The total strain and nominal stress of this cell is then considered in a manner similar to uniform averaged stresses and strains of conventional finite elements.

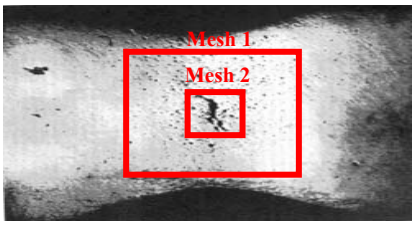

Fig. 1: Necking of a copper tensile specimen with profusion voids and central crack (from Garrison and Moody, 1987)

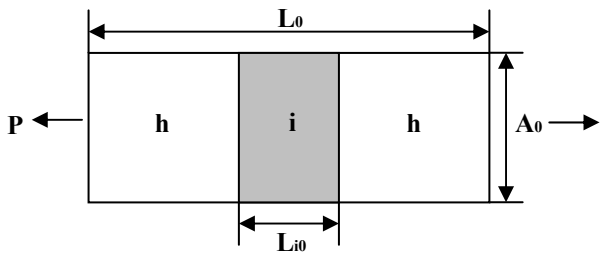

Fig. 2: Three-piece-cell

The fracture strain will be mesh-independent if the material is ideally incompressible and perfectly homogeneous. However, there are always imperfections within the material and strain localization is often concentrated at sites such as micro voids, inclusions and cracks etc. The parameter we use to describe the size of the imperfect part is defined as:

$$\lambda = \frac{L_{i0}}{L_0} \tag{1}$$

where, L_{i0} is the characteristic size of microscale material imperfection, considered here a material property. L_0 is the initial length of the whole cell, (it thus directly describes mesh size). Equation (2) is derived (Li, 2006, Li and Karr 2007b) by using compatibility conditions, which is satisfied until fracture occurs.

$$e^{\varepsilon_{total}} = (1-\lambda)e^{\varepsilon_h} + \lambda e^{\varepsilon_i} \tag{2}$$

where, ε_{total} is the total true strain of the cell, ε_h and ε_i are the true strains in the homogeneous piece and imperfect piece, respectively.

For the multi-piece-cell, which is more realistic than the three-piece-cell, the total fracture strain of the whole cell will be

$$\varepsilon_{total} = \ln(\sum_{1}^{m} \lambda_i e^{\varepsilon_i}) \tag{3}$$

where, λ_i and ε_i is the geometric parameter and true strain in each part.

Rearranging equations (1) and (2), the quantitative relation between the strains within the homogeneous and imperfect part at fracture is

$$\varepsilon_f(f,\lambda,n) = \ln(\frac{a}{L_0} + b) \tag{4}$$

where:

$$\begin{cases} a(f,n) = (e^{\varepsilon_i^*} - e^{\varepsilon_h^*})L_{i0} \\ b(f,n) = e^{\varepsilon_h^*} \end{cases} \tag{5}$$

and where $\varepsilon_h^*, \varepsilon_i^*$ are true strains at fracture in the homogeneous part and imperfect part respectively and can be determined by constitutive bifurcation criteria, either one-dimensional or multiple-dimensional. For one-dimensional stress control loading conditions, it corresponds to the maximum load with strains concentrated in the imperfection zone. Also, f represents the size of imperfection and n is the material property index for the power law plasticity equation $\sigma = K\varepsilon^n$.

Size effects for power law plastic material

For incompressible power law plasticity, where n is the index, the quantitative relation between the strains within the homogeneous and imperfect parts is:

$$\varepsilon_h^{\,n} e^{-\varepsilon_h} = (1-f)\varepsilon_i^{\,n} e^{-\varepsilon_i} \tag{6}$$

Here, the parameter f is the size of the geometric imperfection of the three-piece cell, representing the cross section area reduction. It can be shown, with $f = 0$, that the maximum nominal stress is $\sigma / K = n^n$ obtained at $\varepsilon_i = n$. This

is the Considère criterion (see also Malvern, 1969). Returning to equation (6), the relationship between ε_i and ε_h can be established for various values of f. For nonzero values of f, the curves contain turning points where the strain in the imperfect zone increases and the strain in the homogeneous portions decreases, hence indicating the localization of strain and the onset of fracture. This is shown in Fig.3 where the bifurcation strains or fracture points are obtained as:

$$\begin{cases} \varepsilon_i^* = n \\ \varepsilon_h^* = \varepsilon_h^*(f,n) = -nLambertW[-(1-f)^{\frac{1}{n}}] \end{cases} \quad (7)$$

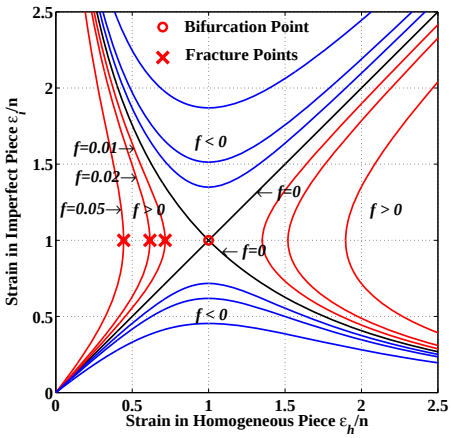

Fig. 3: Fracture points determined by Strain Bifurcation Diagram for different geometric imperfections

The 'LambertW' in equation (7) represents the Lambert W function, which has the form $W(z)e^{W(z)} = z$ (see for example Corless, et al., 1996). Substituting equation (7) into equation (5) and equation (4), the influence of the geometric imperfection f and the material hardening index n on the size effects can be obtained. Shown in Fig. 4 are the effects of varying f.

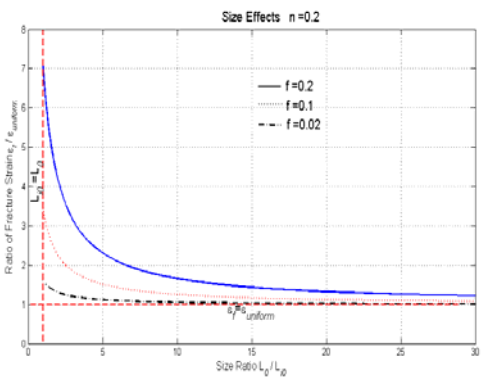

Fig. 4: Effects of imperfection size on the ratio of fracture strains for various values of the area ratio.

The size effects predicted by equation (4), (5) are compared with the FEM analysis performed by Li et al. (2002). Since the micro parameters of the material are not known, we use the least square method with two parameters (a and b) optimization to fit the curve from the FEM analysis, see Fig. 5. The trend is captured by these formulae. If the micro scale parameters are known, equations (4) and (5) provide a quantitative relation to predict the fracture strain input in FEM analysis for given mesh size of the FE model.

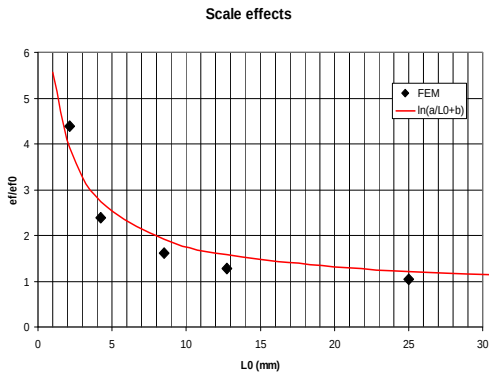

Fig. 5: Comparison between FEM results and analytical relation

Size effects prediction

With the development of tomography technology, the imperfection of the specimen can be measured (Weiler, et al 2005). Thus quantitative prediction of size effects is possible. Die-cast magnesium alloy AM60B samples were examined by Weiler and colleagues with the use of X-ray tomography (Fig. 6). The size and locations of pores in five tensile samples were obtained from the X-ray tomography data. In this section the size effects of AM60B is predicted by using data provided in Weiler's experiments, which is an application of the methodology described above.

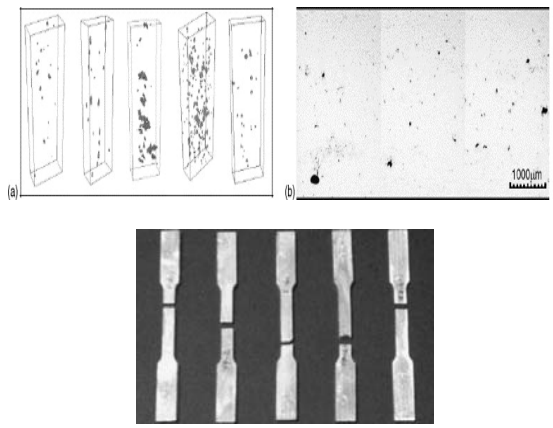

Fig. 6: 3D X-ray image for specimens in Weiler's experiment and image of final fracture (from Weiler et al., 2005)

The yield function of the randomly voided material developed by Gurson (1977) was modified by Tvergaard and Needleman (1984). This function is referred to as the GTN model, which is shown in equation (8).

$$\phi = \frac{\sigma_e^{\ 2}}{Y_m^{\ 2}} + 2q_1 f_g \cosh(q_2 \frac{\sigma_1 + \sigma_2 + \sigma_3}{2Y_m}) - q_3 f_g^{\ 2} - 1 = 0 \qquad (8)$$

Here, Y_m is the flow stress of the matrix material, σ_i are the principal values of the Cauchy stress, and f_g is the current volume fraction of voids. For spherical voids, $q_2 = 1$, and for cylindrical voids $q_2 = \sqrt{3}$. The incremental constitutive relation is developed by Needleman and Triantafyllidis (1978) as follow:

$$\dot{\sigma}_i = C_{ij}(E_{ij}, Y_m, \dot{Y}_m, f_g, \dot{f}_g, \sigma_i)\dot{\varepsilon}_j \qquad (9)$$

where:

$$C_{ij} = E_{ij} - \frac{E_{ik}\phi_{,\sigma_k} E_{lj}\phi_{,\sigma_l}}{\phi_{,\sigma_i}(\phi_{,Y_m}\dot{Y}_m / \dot{\varepsilon}_i^{\ p} + \phi_{,f}\dot{f} / \dot{\varepsilon}_i^{\ p}) + \phi_{,\sigma_i} E_{ij}\phi_{,\sigma_j}} \qquad (10)$$

For plastic loading

$$\phi_{,\sigma_i}\dot{\sigma}_i > 0 \qquad (11)$$

The stress strain curves and fracture stresses and strains were obtained from Weiler, et al's test of simple tension. In this section, the fracture strains and stresses predicted by GTN model are compared with those obtained from the experiments.

We use the cross section with the largest pores to serve as the imperfection portion in the model. Since the samples were thin, the area porosity is set equal to the volume porosity and the GTN model is used. For samples 1, 2, 3 and 4 the porosities in the imperfection regime are 0.0075, 0.0165, 0.04, and 0.062, respectively; and the porosities in homogeneous regime are 0.001, 0.002, 0.007 and 0.013, respectively. The stress strain relation from the experimental data approximately follows the power law with hardening exponent n=0.14, this value is used for the matrix of all samples. Fig. 7 shows that, with the parameter q_1 = 1.9, the modified Gurson model can predict the fracture strain and fracture stress accurately.

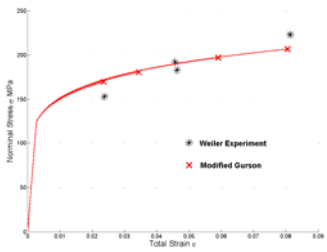

Fig. 7: Comparison of fracture stress and strain predictions and test results

Since the specimens used in Weiler's experiment were of constant length, the size effects are not obvious. However, if one was to simulate the results of the experiments using the finite element method, size effects do arise. To simulate the experiments, we model the cross section with largest pore to extend to a homogeneous zone with length 1mm encompassing the entire width and thickness of the sample and located at the center. The volume porosity of this zone remains unchanged at 0.062. All the material properties outside this zone are the same as before. Also, 1/8 of the specimen is used in a finite element model with mesh size 0.5mm, shown in Fig. 8. Shear free end and axial symmetric boundary conditions are used to simulate simple tension.

Four 'elements' of different sizes with the same size of imperfection are studied. The size of the 'elements' are 3mm, 6mm, 12mm and 25mm separately. The total strain of these models when fracture occurs is considered the "strain to failure" of the 'elements'. A porous plastic constitutive model is used in the simulation using the computer program ABAQUS (2004).

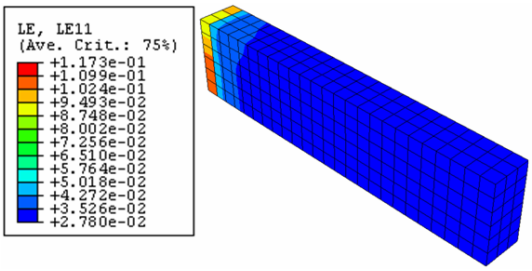

Fig. 8: ABAQUS for strain localization

The constitutive bifurcation in the imperfect zone is used as our fracture criterion. It is predicted by the three-dimensional constitutive bifurcation criteria and the results are shown in Fig. 9, which indicates that $\varepsilon_i^* = 0.115$.

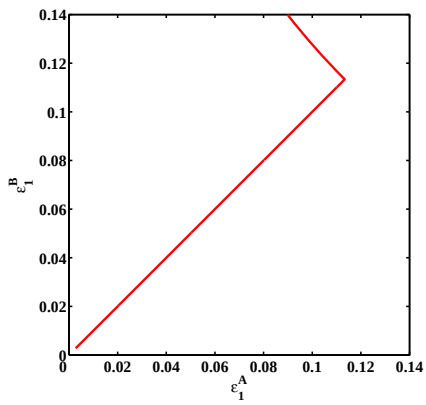

Fig. 9: Constitutive bifurcation in the imperfect zone predicted by the GTN model

Fig. 10 shows that when the displacement of the end of the total FE model reaches 0.395mm, the elements outside the imperfection part begin to unload. This state can be treated as the initiation of fracture in simulation, because normally in a material coupon test, fracture takes place shortly after this point. In the simulation, it is assumed that fracture occurs when the strain in the imperfect part reaches 0.115. For a sample length of 25 mm, the overall average fracture strain is 0.0238 and the data predicted by the GTN model is 0.0236; this corresponds to a strain in the homogeneous portion of

0.0276, which is close to the experimental data of sample 4. The total or overall true strains for different 'element' sizes are shown in Fig. 11 with the evolution of strain in the imperfect part. The corresponding fracture strain can be read from Fig. 11 and is plotted in Fig. 12.

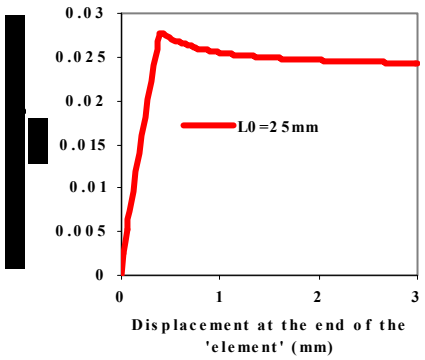

Fig. 10: Relation of displacement and strain

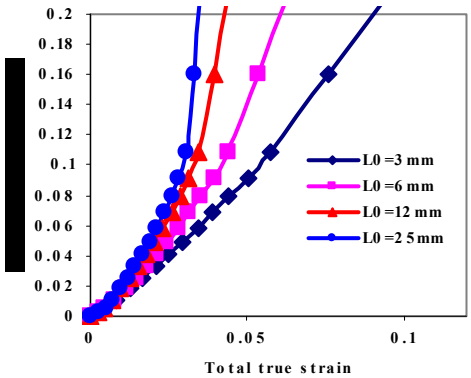

Fig. 11: Total strain and strain in imperfect zone outside the imperfect zone

Using equations (4) and (5), with $L_{i0} = 1mm$, $\varepsilon_i^* = 0.115$, $\varepsilon_h^* = 0.0276$, The size effect is predicted by the solid line in Fig. 12. Very nice agreement with the results from the finite element analysis is shown in Fig. 12.

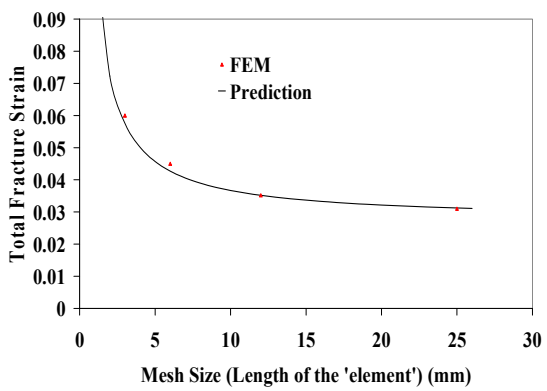

Fig. 12: Comparison of size effects obtained from FE simulation and Prediction by equation (4) and (5)

Recent studies of the fracture of structural steels also emphasize the importance of characteristic length parameters. Material tests and analyses of mild, low-carbon steels were presented by Kanvinde and Deierlein (2006). They used both void growth and stress modified critical strain models for several steels. When incorporated in finite element models to simulate fracture of steel structures, a critical average value of strain is to be achieved over a volume of material to form a crack. The question again arises as to the size of the critical volume. Note that in some applications, the finite elements may generally be smaller than the critical volume, also expressed by the characteristic length l^*.

This issue is addressed also by Chi, Kanvinde and Deierlein (2006). Material specific parameters for A572 Grade 50 steel were found using notched tensile tests. Results of the tests were analyzed using the finite element method and fracture predictions based on various levels of characteristic lengths of .09mm, .20mm and .38 mm, with the upper and lower limits being estimates based on the material substructure. Their approach was to simulate fracture based on a given stress modified critical strain. The predicted end displacement at fracture increased as the characteristic length increased. Using the data provided in Table 1 presented by Chi et al., we reduced the critical strain to failure as the characteristic length increased in accordance with equation (4). Excellent agreement is found by applying this approach to the results of the three point bending tests and compact tension tests of Table 1 of Chi et al., as presented in Figure 13. In the figure, we have normalized the failure strains with respect to the value for the smallest characteristic length and we have used the smallest characteristic length for our L_{i0}.

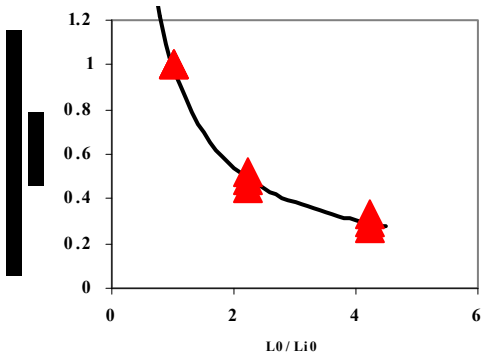

Fig.13: Prediction of Size effects for mild A572 Grade 50 steel

Three-Dimensional Constitutive Bifurcation Criteria for Material Failure

For ideally homogenous material, either compressive or incompressive, there is a critical three dimensional stress-strain state $\sigma_i^*(\dot{\underline{\sigma}}, \dot{\underline{\varepsilon}}, \underline{\varepsilon})$ and $\varepsilon_i^*(\underline{\sigma}, \dot{\underline{\sigma}}, \dot{\underline{\varepsilon}})$, in principal directions, when constitutive bifurcation occurs, in the theory of material instability. Li (2006) proposed three-dimensional constitutive bifurcation criteria for two bifurcation modes: splitting and shear band.

First, we assume fracture is caused by splitting in the direction perpendicular to the principal direction. Consider one cubic cell shown in Fig. 14(a), whose edges are parallel to the local principal directions. Thus the differential equilibrium equations in the local principal coordinates for this cell are first determined. For force equilibrium, we get

$$\Delta(\sigma_i L_j L_k) = 0 \qquad i, j, k = 1,2,3 \qquad i \neq j \neq k \tag{12}$$

where σ_i is one of the principal stresses, L_j, L_k are the

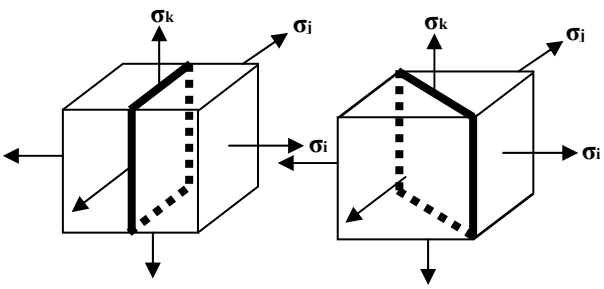

(a) Splitting **(b) Shear band**

Fig. 14: Sketch of bifurcation modes

dimensions of the cubic cell in other two principal directions. Also, Δ represents the difference between the force inside the necking band and that outside it. It functions like a total derivative. Introducing the definition of natural strain:

$$\dot{\varepsilon}_i = \frac{\dot{L}_i}{L_i} \qquad i = 1,2,3 \tag{13}$$

We find from equation (12),

$$\sigma_i L_j L_k \left[\dot{\sigma}_i + \sigma_i (\dot{\varepsilon}_j + \dot{\varepsilon}_k) \right] = 0 \tag{14}$$

For the trivial solution $\sigma_i = 0$, equilibrium equation is satisfied automatically. The non trivial solution is to let the bracket equal to zero, yielding a characteristic equation. Therefore, the characteristic equation for bifurcation is shown in equation (14) which is a general criterion for 3D fracture criteria based on the splitting mode:

$$\dot{\sigma}_i + \sigma_i (\dot{\varepsilon}_j + \dot{\varepsilon}_k) = 0 \qquad i \neq j \neq k \tag{15}$$

It should be noticed that for the strain control loading process, the stress state and state of stress rate depend on the strain state and the state of strain rate, which influence each other by, for example, a particular plastic flow rule. This criterion should be checked in all of the three principal directions to determine which one is satisfied first, then the bifurcation will occur in that direction. This criterion is not constrained by associative flow rule as Drucker's postulate does. Any kind of plastic flow rule can be used. In fact, it can be applied to not only plastic material, but also all kinds of material models in continuum mechanics, either brittle or ductile, elastic or nonelastic. In addition, no assumption of small deformation is made.

The bifurcation point and direction is determined by the current stress state and the state of stress and strain rate. To this point of view, it can also be applied to history dependent constitutive bifurcation. For the one dimensional case, if the incompressibility assumption is used, it is straightforward to show that it coincides with Considére's criterion $d\sigma_1 / d\varepsilon_1 = \sigma_1$, by rearranging equation (14).

Similarly, the 3D general criterion with periodic shear band bifurcation is proposed. In Fig. 14 (b), a unit cubic of material was cut along the principal directions. Assume the bifurcation mode will be a periodical shear band in the i-j plane; k is the direction orthogonal to the i-j plane, where i, j, k are the principal directions. It is assumed that the principal directions inside the shear band are the same as those outside it. Also, t is defined as the thickness in the k direction. Note the following:

$$\Delta(\sigma_i t) = 0 \qquad i = 1,2,3 \tag{16}$$

$$\dot{\sigma}_i + \sigma_i \dot{\varepsilon}_k = 0 \qquad i \neq k \tag{17}$$

This is the three-dimensional characteristic equations for bifurcation within the periodic shear band mode.

The well known bifurcation criteria for simple tension and plane stress biaxial tension for incompressible power law plastic material with isotropic work hardening in sheet metal forming can be derived from the general three-dimensional criteria, too. The final analytical results are shown in Fig. 15, and the numerical results are exactly consistent with the analytical ones. It can be seen for the shear band mode, the triaxiality is always positive, while for necking mode, negative triaxiality can be obtained.

The results from sixteen experiments in Bao's thesis (2003) are also included. As is described in his thesis, all these specimens are made of Al 2024-T351, whose behavior is close to the power law with n = 0.21. Since the experiments are either one-dimensional or two-dimensional, it is expected that the analytical criteria can predict the fracture. The results are also shown in Fig. 15. The analytical criteria derived in this section provide a lower limit to the experimental results.

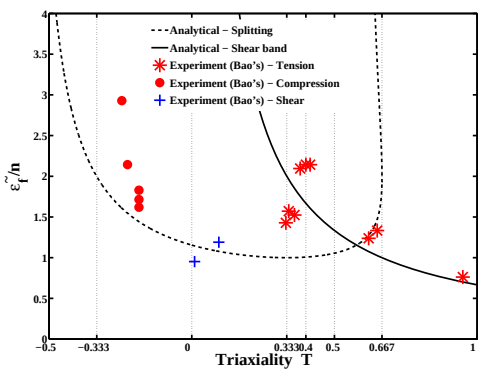

Figure 15: Comparison of analytical results and experimental results for aluminum alloy

For the special case of biaxial tension (plane stress), the shear band criterion simplifies considerably for a power law plastic material with exponent n . As shown in Li (2006) the effective strain to failure is

$$\frac{\tilde{\varepsilon}^*}{n} = \frac{2}{3T} \tag{18}$$

where the triaxiality, T, is defined in terms of the mean and effective stresses by:

$$T = \frac{\sigma_m}{\tilde{\sigma}} \tag{19}$$

This is qualitatively similar in form to the empirical relationships proposed by Kitamura (2001) and Broekhuijsen, 2003 and those shown by Lehmann & Yu 1998.

Conclusions

The relations found for size effect descriptions are derived based on localization models for fracture initiation. We note that these formulae show qualitatively similar relationships to the empirical curves provided by other authors. Our relations are derived for power law plastic materials and are shown to be in approximate agreement with more sophisticated void growth models. For uniaxial analyses, a single formula is presented in terms of the power law exponent, and the ratio of the microscale flaw length to the element length.

A quantitative relation of size effects is proposed, equations (4) and (5), based on a three-piece-cell model. This logarithmic relation catches the trend of mesh size effects observed in finite elements simulation. Different materials have different mesh size effects. With the development of X ray tomography technology, the important microscale material properties are measurable. The imperfection-induced nonuniform strain distribution is the physical reason of mesh size effects. Based on the methodology discussed in this paper, “strains to failure” along the principal directions according to different mesh sizes can be predicted accurately. In addition, it is shown the triaxiality effects can also be included in such analyses when three-dimensional localization models are adopted.

Acknowledgement

Support from the Office of Naval Research through Grant N00014-03-0983 to the University of Michigan is gratefully acknowledged.

References

ABAQUS 2004.User's Manual version 6.5.

Alsos, H. S., Amdahl, J., 2005. Intentional grounding of disabled ships, Marine 2005- Computational Methods in Marine Engineering, Oslo, Norway, 27-29.

Bao, Y. July 2003. Prediction of Ductile Crack Formation in Uncracked Bodies. Ph. D thesis in the Department of Ocean Engineering in MIT.

Bažant, P. Z., 1997. Scaling of Structural Failure. Appl. Mech. Rec. Vol. 50, No.10, 593-620.

Bažant, Z.P., 2000. Size effect, International Journal of Solids and Structures 37, 69-80.

Bažant, Z.P., Guo, Z., 2002. Size effect and asymptotic matching approximations in strain-gradient theories of micro-scale plasticity, International Journal of Solids and Structures 39, 5633-5657.

Broekhuijsen, J., 2003. Ductile failure criteria and energy absorption capacity of the Y-shape test section, Master degree thesis, Technical University of Delft.

Chi, W.-M., Kanvinde, A.M. and Deierlein, G.G., 2006. Prediction of Ductile Fracture in Structural Steel Connections Using SMCS Criterion, J. of Structural Engineering , Feb. 171-181.

Considère, A.G., 1885. Memoire sur l’Emploi du Fer et de l’ Acier dans les Constructions. Annales des Ponts et Chausses, ser. 6 (9), 574-775.

Corless, R.M., Gonnet, G.H., Hare, D.E.G., Jeffrey, D.J., Knuth, D.E., 1996. On the Lambert W Function. Adv. Comput. Math. 5, 329-359.

Engelen, R.A.B., Fleck, N.A., Peerlings, R.H.J., Geers, M.G.D., 2006. An evaluation of higher-order plasticity theories for predicting size effects and localization, International Journal of Solids and Structures 43, 1857-1877.

Flech, N.A., Hutchinson, J.W., 1993. A phenomenological theory for strain gradient effects in plasticity, J. Mech. Phys. Solids 41, No.12, 1825-1857.

Flech, N.A., Hutchinson, J.W., 2001. A reformulation of strain gradient plasticity, Journal of Mechanics and Physics of Solids 49, 2245-2271.

Garrison, W. M. and Moody, N. R. 1987. Ductile fracture. J. Phys. Chem. Solids 48, 1035-1074.

Giovanola, J. H., Kirkpatrick, S. W., 1998. Using the Local Approach to Evaluate Scaling Effects, International Journal of Fracture 92, 101-116.

Gurson, A. L. 1977. Continuum theory of ductile rupture by void nucleation and growth: part I- yield criteria and flow rules for porous ductile media. Transactions of the ASME. J. of Engineering materials and Technology, Jan. 2-15.

Kanvinde, A.M. and Deierlein, G.G., 2006. Void Growth Model and Stress Modified Critical Strain Model to Predict Ductile Fracture in Structural Steels, J. of Structural Engineering , Dec. 1907-1918.

Kitamura, O., 2001. FEM approach to the simulation of collision and grounding damage. Proceeding of 2nd International Conference on Collision and Grounding of Ships, Copenhagen, Dammark,2001.

Lee, Y. W., Wierzbicki T. , 2005. Fracture prediction of thin plates under localized impulsive loading. Part I: dishing,

International Journal of Impact Engineering, 31(10): 1253-1276.

Lehmann, E., Yu, X., 1998. On ductile rupture criteria for structural tear in the case of ship collision and grounding, International Symposium on Practical Designs of Ships and Floating Structures (PRADS), The Hague, The Netherlands.

Li, Y.N. 2006. Ductile Fracture due to Localization and Void Growth for 3D Randomly Voided Materials, Ph.D thesis

Li, Y.N., Karr, D. G. (2007a) Study of Uniaxial Tension from a New Point of View (Submitted to International Journal of Nonlinear Mechanics)

Li, Y.N., Karr, D. G. (2007b) Prediction of Ductile Fracture in Tension by Bifurcation, Localization, and Imperfection Analysis, (Submitted to International Journal of Plasticity)

Li, Y.N., 2003. Study on Nonlinear Finite Element Simulation of Ship-bridge Collision, Master Degree thesis (in Chinese).

Li, Y.N., Gao, Z. and Gu, Y., 2002. The Benchmark Study of the Tensile Coupon Test and Model Test of Ship Grounding. Journal of Ship Engineering 6, 13-17. (in Chinese)

Malvern, L. E. 1969. Introduction to the Mechanics of a Continuous Medium. by Prentice-Hall, Inc. Englewood Cliffs, N. J.

McClintock, F. A. 1968. A criterion for ductile fracture by the growth of holes, J. Appl. Mech. Jun., 363-371.

McClintock, F. A. 1971. Plasticity aspects of fracture. In “Fracture” (Liebowitz, H. Ed.), Academic Press, New York.

Needleman, A. and Triantafyllidis, N. 1978. Void Growth and Local Necking in Biaxially Stretched Sheets, Transactions of the ASME 100, 164-169.

Needleman, A., Tvergaard, V., 1984. An Analysis of ductile rupture in notched bars. J. Mech. Phys. Solids32 (6), 461-490.

Okazawa, S., Fujikubo, M. and Hiroi, S., 2004. Static and dynamic necking analysis of steel plates in tension, Third International Conference on Collision and Grounding of Ships (ICCGS), Izu, Japan, 25-27.

Paik, J. K. 2003. ISSC V.3 Committee Collision and Grounding, ISSC, San Diego, CA.

Kuroiwa, T., Kawamoto, Y. and Yuhara., T., 1992. Study on damage of ship bottom structure due to grounding. The Conference on Prediction Methodology of Tanker Structural Failure.

Rice, J. R. and Tracey, D. M. 1969. On the Ductile Enlargement of Voids in Triaxial Stress Fields. J. Mech. Phys. Solids, Vol. 17, 201-217.

Servis, D., Samuelides, M., Louka, T. and Voudouris, Giorgos, 2001. The implementation of finite element codes for the simulation of ship-ship collisions. Proceeding of 2nd International Conference on Collision and Grounding of Ships, Copenhagen,Danmark.

Simonsen, B. C., Tornqvist, R., 2004. Experimental and numerical modeling of ductile crack propagation in large-scale shell structures, Marine Structures 17, 1-27.

Wang, G. 2006. ISSC V.1 Committee Collision and Grounding, ISSC, Southampton, UK.

Weiler, J.P., Wood, J.T., Klassen, R.J., Maire, E., Berkmortel, R. and Wang, G., 2005. Relationship between internal porosity and fracture strength of die-cast magnesium AM60B alloy. Material Science and Engineering A 395, 315-322.

Yamada, Y., Endo, H., Pedersen, P. T., 2005. Numerical study on the effect of buffer bow structure in ship-to-ship collisions, International Offshore and Polar Engineering Conference (ISOPE), Seoul, Korea, 19-24.